Controlling surface contact, oxygen transport, and pitting of surface oxide via single-channel scanning electrochemical cell microscopy

Li, Yuanjiao; Morel, Alban; Gallant, Danick; Mauzeroll, Janine

Publisher's version / Version de l'éditeur:
https://doi.org/10.1021/acs.analchem.2c02459
Analytical Chemistry, 94, 42, pp. 14603-14610, 2022-10-10

analytical chemistry

pubs.acs.org/ac Article

Controlling Surface Contact, Oxygen Transport, and Pitting of Surface Oxide via Single-Channel Scanning Electrochemical Cell Microscopy

Yuanjiao Li, Alban Morel,* Danick Gallant,* and Janine Mauzeroll*

Cite This: *Anal. Chem.* 2022, 94, 14603−14610 Read Online

ACCESS | Metrics & More | Article Recommendations | Supporting Information

ABSTRACT: In single-channel scanning electrochemical cell microscopy, the applied potential during the approach of a micropipette to the substrate generates a transient current upon droplet contact with the substrate. Once the transient current exceeds a set threshold, the micropipette is automatically halted. Currently, the effect of the approach potential on the subsequent electrochemical measurements, such as the open-circuit potential and potentiodynamic polarization, is considered to be inconsequential. Herein, we demonstrate that the applied approach potential does impact the extent of probe-to-substrate interaction and subsequent microscale electrochemical measurements on aluminum alloy AA7075-T73.

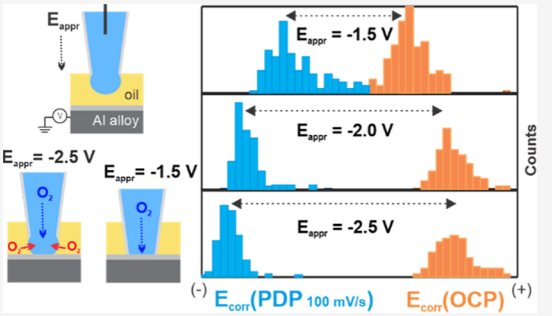

1. INTRODUCTION

Scanning electrochemical cell microscopy (SECCM) enables direct electrochemical measurements at microscopic sites by scanning a droplet cell over a substrate surface.[1−3] The droplet landing on the substrate is the key step in SECCM experiments, the mechanism of which varies with the types of pipettes. In the two-channel pipette system,[2,4,5] a bias potential is applied between two quasi-reference counter electrodes (QRCEs), producing a conductance current (i_c) between the two channels. The pipette is oscillated, giving rise to an alternating component of the i_c, which is used as the feedback signal for droplet landing. In the single-channel SECCM, a potential (E_{appr}) is applied during the approach of the micropipette to the substrate. A transient current (i_{trig}) is produced when the droplet makes contact with the substrate, triggering the pipette to stop moving down.[6,7] Other droplet landing feedback signals are also reported in the single-channel system, such as fear force,[8,9] alternating current,[10] and potential.[7,11] These need more complex equipment or elaborate operations to support them.

Due to the ease of operation, single-channel SECCM using the direct transient current (i_{trig}) as the feedback signal has been widely used in various fields.[6,12−18] Recently, it was introduced into the field of metal corrosion for the exploration of the microstructure feature-related corrosion activities.[19−23] To gain insight into the microscopic electrochemical measurements in the SECCM experiments, the current and potential changes due to the droplet landing process were analyzed from the E_{appr} perspective.

In the single-channel pipette system, i_{trig} must have a higher magnitude than the background noise, which is the minimal threshold; otherwise, the micropipette will not stop until the tip glass makes contact with the substrate. For a given micropipette diameter, the magnitude of i_{trig} depends on the conductivity of the substrate, the composition of the electrolyte, and E_{appr}. Since the substrate and electrolyte are often experimentally fixed, the magnitude of i_{trig} is primarily controlled by E_{appr}. For conductive substrates or electrolytes containing active redox species, such as carbon-based materials,[24,25] battery materials,[6,26−30] Au,[16,18,31] Pt,[6,10] Fc/Fc$^+$,[32] $[Fe(CN)_6]^{2+/3+}$,[1] and $[Ru(NH_3)_6]^{2+/3+}$,[7,33] it is easy to achieve a i_{trig} higher than the current threshold despite applying a small E_{appr}. For example, an E_{appr} of 0.65 V (vs Ag/AgCl) applied to a $LiFePO_4$ composite electrode gave rise to a i_{trig} up to 9 pA (threshold = 2 pA) upon contact with a droplet cell at the end of a 100 nm diameter pipette.[6] An E_{appr} of −200 mV (vs the reversible hydrogen electrode (RHE)) applied on a conductive noble graphene substrate generated a capacitive current high enough to trigger a 70 nm diameter pipette filled with 0.5 M H_2SO_4 to stop upon the droplet contact with the graphene substrate.[24]

When studying corroding alloys, the electrolytes typically do not contain added active redox species since they will influence the corrosion mechanism. i_{trig} is mainly dependent on corrosion reactions such as metal dissolution and oxygen

Received: June 8, 2022
Accepted: September 26, 2022
Published: October 10, 2022

https://doi.org/10.1021/acs.analchem.2c02459
Anal. Chem. 2022, 94, 14603−14610

reduction reactions (ORR), but the concentrations of reactants are typically low compared to other systems.[6,24,28,31] Additionally, i_{trig} is expected to have a lower magnitude on passive metals compared to conductive substrates due to the presence of surface oxides that reduce the surface conductivity.[34,35] Single-channel SECCM measurements on Zn,[21] Cu,[11] and low-carbon steel,[19,20] have been reported, but they used acidic electrolytes, in which the corrosion of substrates was more aggressive than in neutral electrolytes. In such cases, a sufficiently large i_{trig} is easy to achieve. In fact, the effects of E_{appr} are present to varying degrees depending on the substrates but have never been elucidated,[22] probably because it was considered to be innocuous to subsequent microscopic electrochemical measurements.

We systematically analyzed the effects of E_{appr} on the microscale open-circuit potential (OCP) and potentiodynamic polarization (PDP) measurements on an Al alloy AA7075-T73 in the oil-immersed single-channel micropipette SECCM.[11,21,23] Due to the presence of a barrier oxide film, the Al surface is less reactive. E_{appr} is thus decisive for the production of a sufficiently large i_{trig} and droplet landing. We demonstrate that E_{appr} controls the extent of micropipette−substrate interactions, impacting the subsequent microscale measurements of corrosion potential (E_{corr}) and the pitting density.

2. EXPERIMENTAL SECTION

2.1. Chemicals and Materials. Sodium chloride (NaCl, anhydrous, 99.8%) and mineral oil (M5310) were purchased from Sigma-Aldrich. Al alloy AA7075-T73 was supplied by the National Research Council (NRC, Canada, Saguenay). A 3.5 wt % NaCl electrolyte solution was prepared using ultrapure water (Milli-Q Reference Water Purification System, Millipore, 18.2 MΩ cm resistivity at 25 °C).

Single-channel micropipettes were fabricated from quartz glass capillaries (Sutter Instrument, Novato, CA) with dimensions of (o.d./i.d.) 1.0/0.3 mm, using a CO_2-laser puller (P-2000, Sutter Instruments, USA). Pulling parameters for a ∼2 μm diameter opening pipette: line 1: heat = 585, filament = 2, velocity = 30, delay = 130, pull = 30. Pulling parameters for a ∼10 μm diameter opening pipette: line 1: heat = 750, filament = 4, velocity = 10, delay = 130, pull = 4. After pulling, the diameter of the tip opening was estimated from the optical image and a more precise value can be measured from the scanning electron microscopy (SEM) image (Figure S1).

An Ag/AgCl wire was prepared by chemically coating a 0.125 mm diameter Ag wire (Goodfellow Metals, Huntingdon, England) with a AgCl film in the household bleach (Clorox, Canada).[36−39] The main gradient of bleach is NaOCl, which oxidizes Ag into AgCl. The stability and reproducibility of the bleach oxidized Ag/AgCl electrode have been demonstrated in our previous work.[39] Note that, unless otherwise specified, all potentials reported below have been calibrated to the Ag/AgCl wire in the 3.5 wt % NaCl solution, which has a 5 mV difference with respect to the saturated calomel electrode (SCE).

Glassy carbon (GC) was successively polished with 1, 0.3, 0.1, and 0.05 μm-diameter alumina powder (Struers, USA) on polishing clothes (Struers, Canada), followed by sonication in ultrapure water before drying in air.

2.2. Aluminum Alloy Sample Preparation and Surface Characterization. Al alloy AA7075-T73 was polished with a 320 grit SiC paper (Struers, Canada), followed by 9 and 3 μm colloidal diamond suspensions (Struers, Canada), on a MD Chem cloth pad (Struers, Canada), using a TegraPol-25 polishing wheel (Struers, USA). A mirror-like surface was achieved after the final polishing step by employing a colloidal silica suspension (Struers, Canada) on the MD Chem cloth. The sample surface was then rinsed with anhydrous ethanol and sonicated in ultrapure water for the removal of the residuals of silica suspensions before drying in air. The sample was fixed in a cell holder (Figure S2), in which a layer of mineral oil was added on the surface of the sample for oil-immersed SECCM.

The surfaces were imaged by an optical microscope and SEM (FEI Helios Nanolab 660 dual beam, 5 keV). The surface topography was scanned by atomic force microscopy (AFM) with a molecular force probe controller (Asylum Research-an Oxford Instruments Company, Santa Barbara, CA) equipped on an MFP3D microscope working in alternating contact mode in air. The cantilevers were model ACTA (AppNano, Mountain View, CA).

2.3. Macro-PDP Measurements. Macro-electrochemical measurements were conducted using a multichannel VSP-300 potentiostat (BioLogic Science Instruments, USA). The polished samples were mounted in a corrosion cell (K0235 Flat Cell, Princeton Applied Research, AMETEK Scientific Instruments) with an area of 1 cm^2 exposed to a 3.5 wt % NaCl electrolyte solution. A SCE and platinum mesh served as the reference and counter electrode. Prior to PDP measurement, OCP was measured for 20 min, allowing the corrosion system to reach a stationary state where E_{corr}(OCP) was obtained. The PDP measurement was carried out in the range of E_{corr}(OCP) ± 250 mV at a scan rate of 0.167 mV/s in the positive direction (from negative to positive potentials). A current exceeding the set current limit (10 mA) ended the potential sweep.

2.4. Oil-Immersed Single-Channel Micropipette Scanning Electrochemical Cell Microscopy. Since the 3.5 wt % NaCl solution evaporates rapidly in air, SECCM was carried out under mineral oil as previously reported to prevent the crystallization of the droplet at the end of the micropipette.[11,21,23,39] All electrochemical measurements were performed using an EIProScan 3 system (HEKA, Germany; bipotentiostat model PG340) in a Faraday cage (Acoustic Isolation Novascan Ultracube, Ames IA, USA) on a vibration isolation table (Micro 60 Halcyonics Active Vibration Isolation Platform, Novascan, Ames IA, USA). A micropipette was filled with the 3.5 wt % NaCl electrolyte using a microneedle, as shown in Figure S3. A Ag/AgCl wire was inserted from the top of the micropipette serving as a QRCE. The substrate surface was covered with a thin layer of mineral oil, sufficient to submerge the droplet at the end of the micropipette throughout the experiment. The micropipette was brought to the working electrode (WE) substrate under oil at a rate of 1 μm/s with 1 nm data sampling while E_{appr} was applied. Once the movement of the micropipette was triggered to stop, OCP (30 s) followed by PDP (from −1.3 to −0.3 V at a scan rate of 100 mV/s) measurements were carried out in the established droplet cell.

3. RESULTS AND DISCUSSION

3.1. E_{appr} Determines the Type of Landing. Depending on the choice of E_{appr}, two types of landings were observed, droplet contact (DC) landing and pipette contact (PC) landing, as shown in Figure 1a,b. E_{appr} was selected in the

https://doi.org/10.1021/acs.analchem.2c02459
Anal. Chem. 2022, 94, 14603−14610

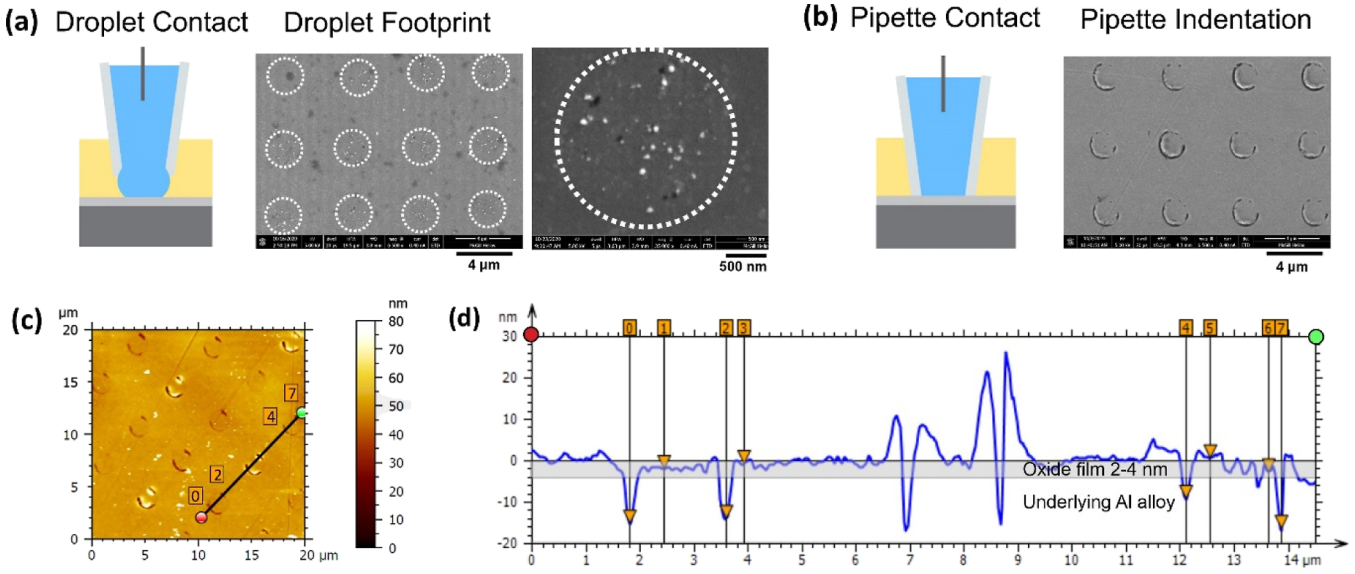

Figure 1. SECCM-scanned surfaces of Al alloy AA7075-T73: (a) corrosion products left by DC landings and (b) indentations left by PC landings. (c) AFM topographic map of the Al alloy surface with PC landings. (d) Line scan across the indentations of three PC landings.

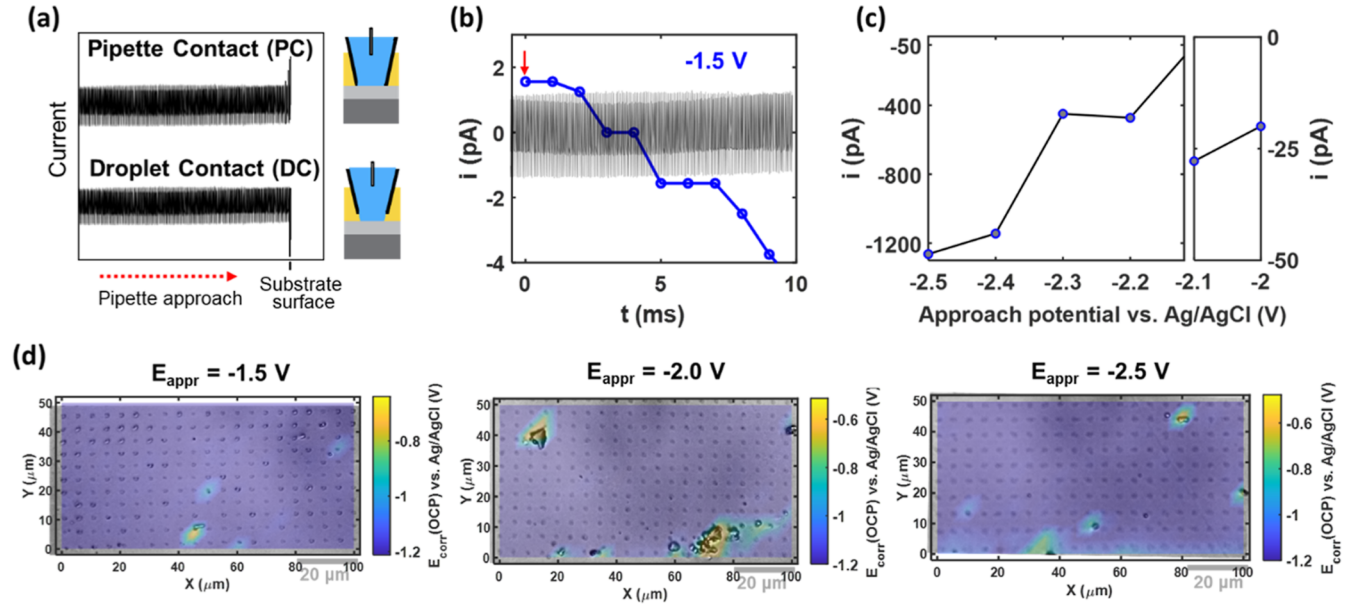

Figure 2. (a) Currents recorded during the process of the micropipette approach to the substrate for the PC (upper curve) and DC landings (lower curve). (b) Chronoamperometry was carried out at an approach potential of −1.5 V for 10 ms immediately after the micropipette made contact with the Al alloy AA7075-T73. The first recorded current pointed by the red arrow was approximated to be i_{trig}. The black trace represents the background noise under the experimental conditions at that time. (c) First current points measured upon landing (i_{trig}) in chronoamperometry were plotted as a function of approach potentials. (d) E_{corr}(OCP) maps of AA7075-T73 generated by SECCM with different E_{appr} were superimposed on optical microscopic images of the scanned surfaces.

cathodic region, more negative than E_{corr}, to prevent significant metal dissolution and morphological changes during SECCM. The E_{corr} of pure Al (−1.329 V, Figure S4) was used as an approximation for the Al alloy matrix area. DC landings were obtained at E_{appr} of −2.5 V. Figure 1a shows white particles left by the droplet on the alloy surface, which identified the area of DC landing. PC landings obtained at an E_{appr} of −1.5 V left dark circles on the alloy surface (Figure 1b), which were consistent with the size of the tip opening of a ∼2 μm diameter micropipette. The pipette indentations were confirmed by AFM mapping (Figure 1c,d). A line scan over three landings is displayed in Figure 1d to quantify the indentation depth. At locations 0 and 2, the depths are 13.24 and 13.23 nm, respectively, exceeding the usual oxide film thickness (∼2−4 nm),[40,41] which indicates that the pipette physically damaged the oxide film. Most of the indentations in Figure 1c are actually not full circles and are crescent-shaped in some cases. This is attributed to the tilt of the micropipette opening relative to the alloy surface.

The formation of DC and PC landings was tied to the magnitude of i_{trig}, which determined when the approach of the micropipette was stopped. Positive and negative i_{trig} were observed for PC and DC, respectively (Figures 2a and S5). To elucidate the landing process, i_{trig} was measured at different

https://doi.org/10.1021/acs.analchem.2c02459
Anal. Chem. 2022, 94, 14603−14610

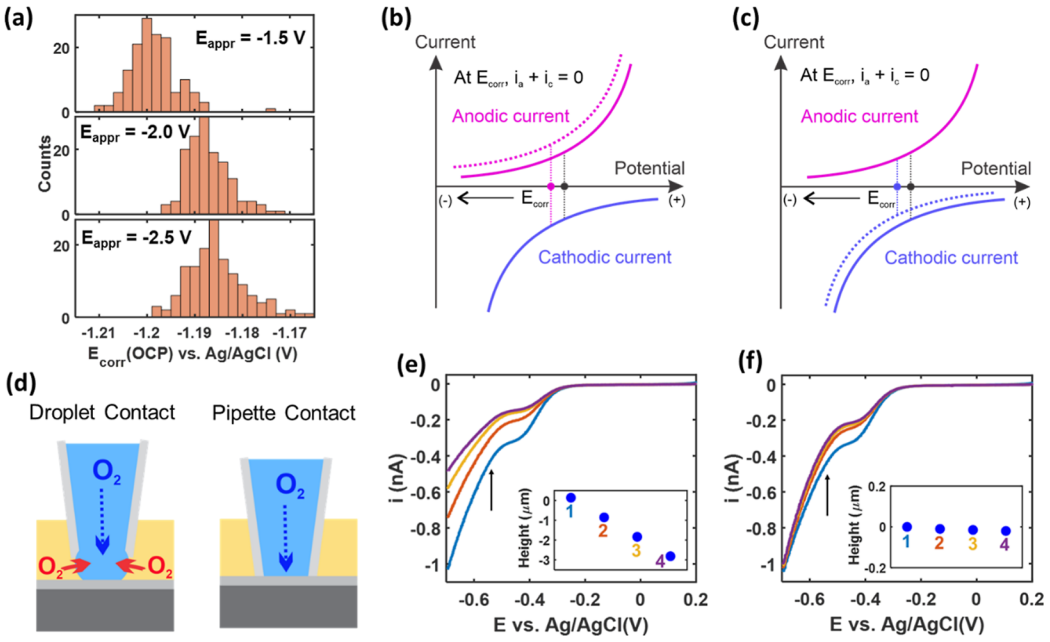

Figure 3. (a) Histograms of E_{corr}(OCP) obtained from the SECCM maps in Figure 2d at different E_{appr}. (b) Anodic current increase and (c) cathodic current decrease induce the negative shift of E_{corr} according to the mixed potential theory. (d) Oxygen fluxes to the metal−electrolyte interface at the DC and PC landings. Red arrows represent the oxygen flux from the oil phase to the droplet. The blue arrows represent the oxygen flux from the bulk solution along the micropipette. (e) Cathodic polarization measurement of the ORR was carried out at a scan rate of 100 mV/s upon a DC landing on the surface of GC in SECCM. The droplet was formed at the end of a 3.5 wt % NaCl solution-filled 10 μm-diameter micropipette. DC landing was obtained at −1.5 V E_{appr} (Figure S7). After the first ORR curve, the micropipette was moved down 1 μm three consecutive times to diminish the droplet−oil interface followed by an ORR measurement each time. (f) ORR measurements were repeated four times without further lowering the micropipette once the droplet landed on GC. The arrow shows the sequence of ORR measurements.

E_{appr} with chronoamperometry carried out on the Al alloy using a 2 μm diameter micropipette. The first current point on the chronoamperogram curve was approximated to be i_{trig}. For PC landings obtained with a −1.5 V E_{appr}, the current was positive at the first point (red arrow in Figure 2b) and then progressively became negative with time. Theoretically, the cathodic potential of −1.5 V should produce a negative current. The positive current could be the current noise made by the physical contact between the micropipette and alloy or an anodic current of the oxidation of the freshly exposed underlying Al due to the PC damaging the oxide film. We infer that the DC-produced i_{trig} was smaller than the current threshold and thus could not stop the micropipette approach. Consequently, the micropipette continued moving down until PC generated a positive current to trigger the micropipette to stop. Accordingly, to obtain DC landings, a more negative E_{appr} is needed to generate a larger i_{trig}. Figure 2c shows the increase of i_{trig} (absolute value) with E_{appr} from −2 to −2.5 V. With respect to a current threshold of 2 pA shown by the amplitude of the background noise in Figure 2b, the i_{trig} values at E_{appr} from −2 to −2.5 V are sufficient to produce DC landings. It must be noted that the droplet was brought near the substrate at a small rate (−1 μm/s) considering the time needed for the droplet to rupture the oil before it makes contact with the substrate.[42] A high approach rate caused PC landings even at the −2.5 V E_{appr} (Figure S6). Comparing the landings at different approach rates and E_{appr} values (Figure S6), we demonstrated that at a fixed rate, E_{appr} determined the types of landings.

Although the PC landings damaged the oxide film, the E_{corr}(OCP) map (−1.5 V E_{appr}) can still qualitatively display the correlation between the electrochemical activities and the alloy surface microscopic features similar to the maps of DC landings obtained at E_{appr} of −2.0 and −2.5 V (Figure 2d). Moreover, the pipette indentation provides a way to mark the scanned area for post-characterizations. However, from a semiquantitative perspective, the difference in the types of landings and values of E_{appr} leads to variations in the electrochemical measurements, which will be discussed below by comparing the E_{corr}(OCP) and E_{corr}(PDP) extracted from the three maps in Figure 2d.

3.2. Effect of E_{appr} on E_{corr}(OCP). E_{corr}(OCP) collected from SECCM maps exhibit a dependence on E_{appr} (−1.5, −2.0, and −2.5 V) because of the differences between PC and DC landings (Figure 3a). PC landings with E_{appr} at −1.5 V gave rise to more negative E_{corr}(OCP) compared to DC landings obtained at E_{appr} of −2.0 and −2.5 V. According to the mixed potential theory,[43] E_{corr} shifting to more negative values is due to the increase of anodic current (Figure 3b) or decrease of cathodic current (Figure 3c). In DC landings, the presence of the droplet−oil interface allows for additional oxygen flux diffusing from the mineral oil to the droplet (Figure 3d, red arrows).[21,44] However, in PC landings, the oxygen is entirely supplied by the flux along the micropipette in the bulk solution (Figure 3d, blue arrows). Because of the higher oxygen content in mineral oil,[45−47] the droplet−oil interface serves as a reservoir that enhances the mass transport of oxygen to the metal−electrolyte interface, leading to higher cathodic currents.[21]

To verify the enhancement of ORR in the presence of droplet−oil interface, linear sweep voltammetry (LSV) was run in the negative direction on a GC WE confined by the droplet size in SECCM.[48,49] A 10 μm diameter micropipette was used to generate a large droplet convenient for the adjustment of

https://doi.org/10.1021/acs.analchem.2c02459
Anal. Chem. 2022, 94, 14603−14610

droplet height to vary the droplet−oil interface area. The first polarization curve of ORR was recorded upon droplet landing. The micropipette was then moved down by 1 μm three times in succession to reduce the droplet−oil interface area. After each descent, a polarization curve was recorded to show the effect of the reduced area on the ORR current (Figure 3e). The absolute current decreased with the descent of the micropipette, suggesting a decline in the mass transport of oxygen. For comparison, LSV was repeated four times upon the droplet landing without moving the micropipette down further. The polarization curves did not exhibit significant changes except for the first curve where the oxygen concentration was expectedly higher at the beginning (Figure 3f). This proves that the presence of the droplet−oil interface indeed contributes to an increase in the cathodic current, leading to variations of E_{corr}(OCP) between the PC and DC landings.

3.3. Effect of E_{appr} on E_{corr}(PDP). For a large area SECCM map consisting of hundreds to thousands of landings, the applied potentiodynamic methods at each landing point are performed at high potential scan rates.[4,13,50] For example, SECCM maps of AA7075-T73 using positive PDPs were acquired with a scan rate of 100 mV/s. The high scan rate leads to an increase in the anodic current during PDP, which results in a negative shift of E_{corr}(PDP) relative to the E_{corr}(OCP) (Figure 4a).[51] The anodic current-related processes involve electron transfer at the metal−oxide interface and the migration of metal cations within the oxide film that is regarded as the limiting step.[52−55] The migration of metal cations is driven by the high electric field within the oxide film at applied potentials,[56] which is inversely proportional to the thickness of the oxide film. Since the time for the anodic growth of oxide film during PDP is less at a high scan rate, the oxide film would be thinner compared to that at a low scan rate. The electric field strength is thus stronger during a high-scan-rate PDP, which facilitates the migration of cations within the oxide film. As a result, the anodic current is predicted to be higher.[51] Moreover, the potential scanned at a high rate will generate capacitive charging currents that also lead to the increase of anodic current.[57] The increase of anodic current induced by the high potential scan rate leads to E_{corr}(PDP) shifting to more negative values as illustrated in Figure 3b.

The negative shift of E_{corr}(PDP) relative to E_{corr}(OCP) was found to increase as E_{appr} increased to more negative values (Figure 4a). This was due to the increase of anodic currents with more negative E_{appr} (Figure 4b). The Al alloy surface experienced a transient cathodic polarization at E_{appr} upon the DC.[58,59] As E_{appr} increased to sufficiently negative values, hydrogen evolution occurred, increasing the concentration of OH^- at the oxide−electrolyte interface that accelerated the hydration of the oxide film.[60−62] This will lead to a more porous structure, promoting the migration of cations through the oxide film and thus the anodic current.[63,64] Consequently, the negative shift of E_{corr}(PDP) resulting from the high potential scan rate was more pronounced at more negative E_{appr} values (Figure 4a).

The hydration and increased porosity render the oxide film more susceptible to Cl^- attack, promoting pitting.[65,66] During PDP, a current transient was produced when pitting occurred that exceeded the set current limit of 100 pA, ending the potential sweep (Figure 4c, pink curve). In the absence of pitting, the current was lower than 20 pA throughout the anodic potential range (Figure 4c, cyan curve). Thereby, the

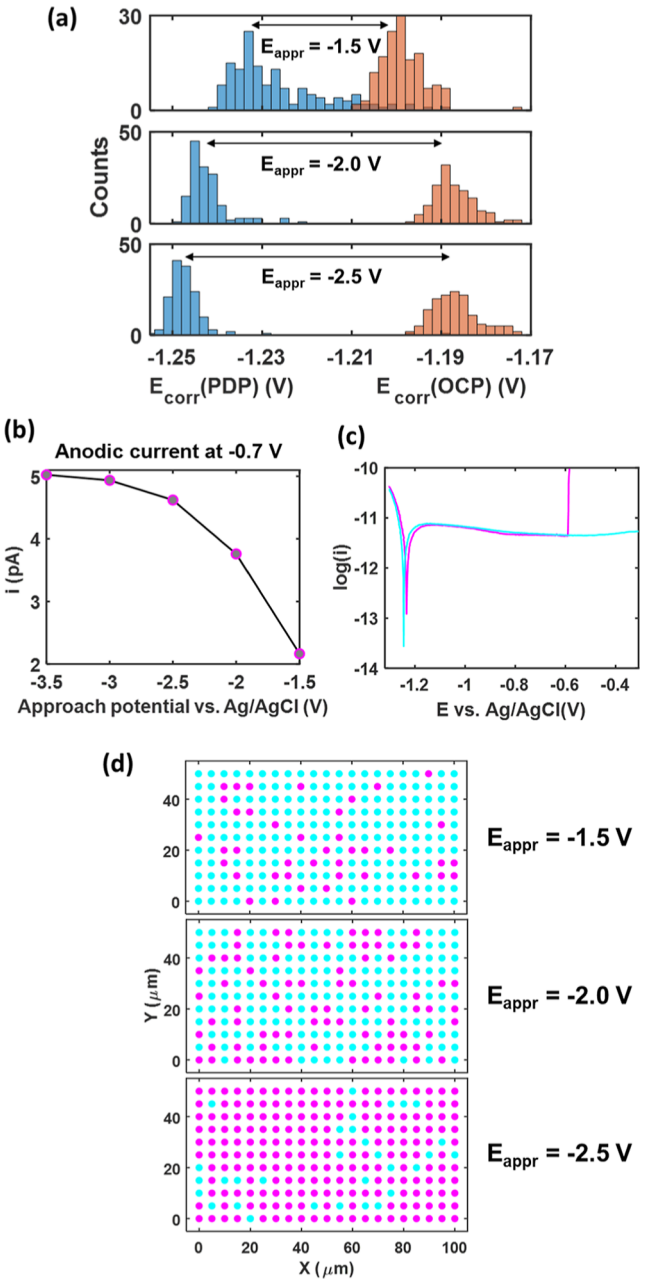

Figure 4. (a) Histograms of E_{corr} measured from OCP and PDP (100 mV/s) measurements in SECCM experiments with different E_{appr}. (b) Averaged anodic currents at −0.7 V extracted from the PDP measurements (Figure S8) at 25 landing locations plotted as a function of E_{appr}. (c) Occurrence (pink) and absence (cyan) of pitting in PDP measurements. (d) SECCM maps of pitting (pink) at different E_{appr}.

magnitudes of the anodic currents at the end of the potential sweep can be used to distinguish the pitting (pink) and nonpitting (cyan) locations on the SECCM maps (Figure 4d). At an E_{appr} from −1.5 to −2.0 V, there was a slight increase in the pitting frequency, whereas at −2.5 V E_{appr}, pitting occurred at a much higher frequency. This implies that the breakdown potential of the oxide film is most likely between −2.0 and −2.5 V under the SECCM experimental conditions. E_{appr} of −2.5 V may have reached the breakdown potential so that pitting readily occurred during PDP. The breakdown potential of the oxide film is not constant, which varies with the anions

https://doi.org/10.1021/acs.analchem.2c02459
Anal. Chem. 2022, 94, 14603−14610

and pH of the solution, thickness, alloying elements of the oxide film, and so on.[64,67,68] This highlights that we can promote the anodic processes by controlling the values of E_{appr}, which increases the anodic current and the frequency of pitting. This is meaningful for the microscopic measurements of the oxide-covered metal surfaces, which produce extremely low currents, making it difficult to discriminate small changes of the surface structure. An important finding of our study is that appropriately increasing the conductivity of the surface oxide by controlling E_{appr} allows us to increase the magnitude of currents without eliminating surface heterogeneity. For example, the difference between matrix and intermetallic particles was maintained even after increasing E_{appr} as shown in Figure 2d. Furthermore, the small difference in electrochemistry between grains can be discerned even by applying a high E_{appr} of −2.5 V (Figure S9), which will be discussed in detail in our ongoing work.

To visualize the impact of E_{appr} on the electrochemical measurements more directly, the PDP measurements at the landings with and without E_{appr} are compared. To facilitate the approach of the micropipette without E_{appr}, a 10 μm diameter micropipette was used. As shown in Figure 5a, an E_{appr} of −2.0 V was applied at one location for the approach and the micropipette was moved up a distance of 15 μm after the PDP measurement. At the subsequent location, the micropipette was moved down 15 μm to obtain a droplet landing without applying E_{appr}. Without E_{appr} being applied, the E_{corr}(PDP) values are more positive (Figure 5b, points on the grid lines) and have negligible shifts with respect to E_{corr}(OCP) (Figure 5c, red points). Additionally, the anodic currents were extremely low (Figure 5d, red points), suggesting the inert property of oxide film, which limits electrochemical measurements at the microscale. In contrast, the application of −2.0 V E_{appr} produced larger anodic currents (Figure 5d, blue points), reflecting the increased conductivity of the surface oxide. This can amplify the small current differences between microstructural variations, which would otherwise be difficult to distinguish between low currents.

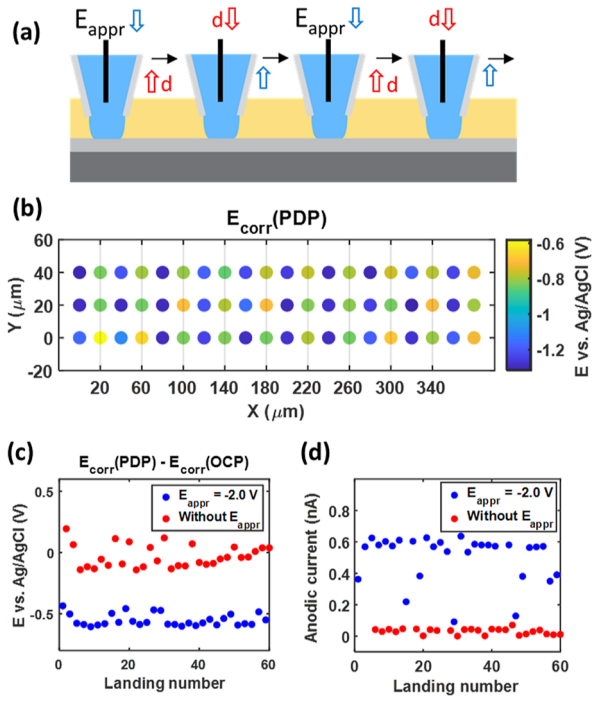

Figure 5. (a) Schematic of the movement of a 10 μm diameter micropipette in the SECCM measurement with E_{appr} applied at every other landing. The micropipette was brought to the AA7075-T73 surface at an E_{appr} of −2 V. After OCP and PDP measurements, the micropipette was moved up a distance of d = 15 μm and then laterally moved to the next spot where the micropipette was moved down at d = 15 μm without E_{appr} being applied. (b) E_{corr}(PDP) maps from the alternately applied E_{appr} SECCM measurement. The points on the grid lines represent the landings without E_{appr} applied. Comparison between the landings with and without E_{appr} being applied: (c) the difference between E_{corr}(PDP) and E_{corr}(OCP); (d) anodic currents at −0.7 V vs Ag/AgCl extracted from PDP curves.

4. CONCLUSIONS

This work demonstrates that the approach potential E_{appr} in SECCM affects the droplet−substrate interaction and the microscale OCP and PDP measurements of Al alloy AA7075-T73. E_{appr} controls the magnitude of the triggering current i_{trig}. A large cathodic E_{appr} generated a high i_{trig}, giving rise to DC landings, while a small E_{appr} resulted in PC landings due to the presence of a passive oxide film on the Al alloy. At DC landings, the droplet−oil interface enhanced the cathodic reaction by introducing additional oxygen flux from the oil phase to the droplet, resulting in more negative E_{corr}(OCP). Additionally, E_{corr}(PDP) values obtained from the positive PDP at 100 mV/s deviated from E_{corr}(OCP) more seriously as the E_{appr} increased to more negative values. This was due to the prior cathodic degradation of the oxide film at E_{appr}, which also accounts for the higher pitting density when more negative E_{appr} values were used. The elucidation of the effect of E_{appr} on the microscale OCP and PDP measurements of Al alloy in the single-channel micropipette SECCM provides a strategy to regulate the electrochemical processes on the metal oxide surface. Controlling E_{appr} can appropriately increase the conductivity of the metal surface oxides and thus the magnitudes of currents but cannot eliminate the surface heterogeneity. This will facilitate the use of small probes to reveal small electrochemical differences on the metal surface, such as between grain orientations.

■ ASSOCIATED CONTENT

Supporting Information

The Supporting Information is available free of charge at https://pubs.acs.org/doi/10.1021/acs.analchem.2c02459.

Additional experimental details including images of the micropipette opening, sample holder cell, microfilling needle, bulk PDP measurement of pure Al, trigger currents of the droplet and PC landings using 2 μm diameter pipettes, optical images of oil-immersed SECCM-scanned surface at different approach rates and E_{appr}, PDP curves at different E_{appr}, trigger currents of DC using a 10 μm diameter pipette, increase of anodic current with more negative E_{appr}, and cathodic current map, as described in Figures S1−S9 in the text (PDF)

■ AUTHOR INFORMATION

Corresponding Authors

Alban Morel − *Automotive and Surface Transportation Research Centre, Division of Transportation and Manufacturing, National Research Council Canada,*

https://doi.org/10.1021/acs.analchem.2c02459
Anal. Chem. 2022, 94, 14603−14610

Aluminum Technology Center, Saguenay G7H 8C3 Quebec, Canada; Email: Alban.Morel@cnrc-nrc.gc.ca

Danick Gallant − *Automotive and Surface Transportation Research Centre, Division of Transportation and Manufacturing, National Research Council Canada, Aluminum Technology Center, Saguenay G7H 8C3 Quebec, Canada*; Email: Danick.Gallant@cnrc-nrc.gc.ca

Janine Mauzeroll − *Department of Chemistry, McGill University, Montreal H3A 0B8 Quebec, Canada*; orcid.org/0000-0003-4752-7507; Email: janine.mauzeroll@mcgill.ca

Author

Yuanjiao Li − *Department of Chemistry, McGill University, Montreal H3A 0B8 Quebec, Canada*

Complete contact information is available at: https://pubs.acs.org/10.1021/acs.analchem.2c02459

Author Contributions

All authors have given approval to the final version of the manuscript.

Notes

The authors declare no competing financial interest.

■ ACKNOWLEDGMENTS

This work was conducted as part of a project funded by the NRC's METALTec industrial research group, the Centre québécois de recherche et de développement de l'aluminium (CQRDA), as well as the Canadian Office for Energy Research and Development (OERD). The authors would like to acknowledge the METALTec industrial research group members and sponsors who supported this investigation and publication.

■ REFERENCES

(1) Williams, C. G.; Edwards, M. A.; Colley, A. L.; Macpherson, J. V.; Unwin, P. R. *Anal. Chem.* **2009**, *81*, 2486−2495.
(2) Ebejer, N.; Schnippering, M.; Colburn, A. W.; Edwards, M. A.; Unwin, P. R. *Anal. Chem.* **2010**, *82*, 9141−9145.
(3) Takahashi, Y.; Kumatani, A.; Shiku, H.; Matsue, T. *Anal. Chem.* **2017**, *89*, 342−357.
(4) Yule, L. C.; Bentley, C. L.; West, G.; Shollock, B. A.; Unwin, P. R. *Electrochim. Acta* **2019**, *298*, 80−88.
(5) Lai, S. C.; Dudin, P. V.; Macpherson, J. V.; Unwin, P. R. *J. Am. Chem. Soc.* **2011**, *133*, 10744−10747.
(6) Takahashi, Y.; Kumatani, A.; Munakata, H.; Inomata, H.; Ito, K.; Ino, K.; Shiku, H.; Unwin, P. R.; Korchev, Y. E.; Kanamura, K.; Matsue, T. *Nat. Commun.* **2014**, *5*, 5450.
(7) Daviddi, E.; Gonos, K. L.; Colburn, A. W.; Bentley, C. L.; Unwin, P. R. *Anal. Chem.* **2019**, *91*, 9229−9237.
(8) Dang, N.; Etienne, M.; Walcarius, A.; Liu, L. *Anal. Chem.* **2020**, *92*, 6415−6422.
(9) Dauphin-Ducharme, P.; Binns, W. J.; Snowden, M. E.; Shoesmith, D. W.; Mauzeroll, J. *Faraday Discuss.* **2015**, *180*, 331−345.
(10) Wang, Y.; Gordon, E.; Ren, H. *Anal. Chem.* **2020**, *92*, 2859−2865.
(11) Daviddi, E.; Shkirskiy, V.; Kirkman, P. M.; Robin, M. P.; Bentley, C. L.; Unwin, P. R. *Chem. Sci.* **2021**, *12*, 3055−3069.
(12) Patel, A. N.; Collignon, M. G.; O'Connell, M. A.; Hung, W. O.; McKelvey, K.; Macpherson, J. V.; Unwin, P. R. *J. Am. Chem. Soc.* **2012**, *134*, 20117−20130.
(13) Takahashi, Y.; Kobayashi, Y.; Wang, Z.; Ito, Y.; Ota, M.; Ida, H.; Kumatani, A.; Miyazawa, K.; Fujita, T.; Shiku, H.; Korchev, Y. E.; Miyata, Y.; Fukuma, T.; Chen, M.; Matsue, T. *Angew. Chem., Int. Ed. Engl.* **2020**, *59*, 3601−3608.
(14) Tarnev, T.; Aiyappa, H. B.; Botz, A.; Erichsen, T.; Ernst, A.; Andronescu, C.; Schuhmann, W. *Angew. Chem., Int. Ed. Engl.* **2019**, *58*, 14265−14269.
(15) Kang, M.; Perry, D.; Kim, Y. R.; Colburn, A. W.; Lazenby, R. A.; Unwin, P. R. *J. Am. Chem. Soc.* **2015**, *137*, 10902−10905.
(16) Bentley, C. L.; Kang, M.; Unwin, P. R. *Anal. Chem.* **2020**, *92*, 11673−11680.
(17) Oseland, E. E.; Ayres, Z. J.; Basile, A.; Haddleton, D. M.; Wilson, P.; Unwin, P. R. *Chem. Commun.* **2016**, *52*, 9929−9932.
(18) Mariano, R. G.; McKelvey, K.; White, H. S.; Kanan, M. W. *Science* **2017**, *358*, 1187−1192.
(19) Yule, L. C.; Shkirskiy, V.; Aarons, J.; West, G.; Shollock, B. A.; Bentley, C. L.; Unwin, P. R. *Electrochim. Acta* **2020**, *332*, 135267.
(20) Yule, L. C.; Shkirskiy, V.; Aarons, J.; West, G.; Bentley, C. L.; Shollock, B. A.; Unwin, P. R. *J. Phys. Chem. C* **2019**, *123*, 24146−24155.
(21) Shkirskiy, V.; Yule, L.; Daviddi, E.; Bentley, C.; Aarons, J.; West, G.; Unwin, P. *J. Electrochem. Soc.* **2020**, *167*, 041507.
(22) Liu, S.; Shi, M.; Zhou, Y.; Li, R.; Xie, Z.; Hu, D.; Zhang, M.; Hu, G. *J. Cult. Herit.* **2020**, *46*, 176−183.
(23) Li, Y.; Morel, A.; Gallant, D.; Mauzeroll, J. *Anal. Chem.* **2020**, *92*, 12415−12422.
(24) Kumatani, A.; Miura, C.; Kuramochi, H.; Ohto, T.; Wakisaka, M.; Nagata, Y.; Ida, H.; Takahashi, Y.; Hu, K.; Jeong, S.; Fujita, J. I.; Matsue, T.; Ito, Y. *Adv. Sci.* **2019**, *6*, 1900119.
(25) Bentley, C. L.; Unwin, P. R. *Faraday Discuss.* **2018**, *210*, 365−379.
(26) Dayeh, M.; Ghavidel, M. R. Z.; Mauzeroll, J.; Schougaard, S. B. *ChemElectroChem* **2019**, *6*, 195−201.
(27) Inomata, H.; Takahashi, Y.; Takamatsu, D.; Kumatani, A.; Ida, H.; Shiku, H.; Matsue, T. *Chem. Commun.* **2019**, *55*, 545−548.
(28) Kumatani, A.; Takahashi, Y.; Miura, C.; Ida, H.; Inomata, H.; Shiku, H.; Munakata, H.; Kanamura, K.; Matsue, T. *Surf. Interface Anal.* **2019**, *51*, 27−30.
(29) Snowden, M. E.; Dayeh, M.; Payne, N. A.; Gervais, S.; Mauzeroll, J.; Schougaard, S. B. *J. Power Sources* **2016**, *325*, 682−689.
(30) Takahashi, Y.; Yamashita, T.; Takamatsu, D.; Kumatani, A.; Fukuma, T. *Chem. Commun.* **2020**, *56*, 9324−9327.
(31) Liu, D.-Q.; Tao, B.; Ruan, H.-C.; Bentley, C. L.; Unwin, P. R. *Chem. Commun.* **2019**, *55*, 628−631.
(32) Payne, N. A.; Mauzeroll, J. *ChemElectroChem* **2019**, *6*, 5439−5445.
(33) Ornelas, I. M.; Unwin, P. R.; Bentley, C. L. *Anal. Chem.* **2019**, *91*, 14854−14859.
(34) Szklarska-Smialowska, Z. *Corros. Sci.* **1998**, *41*, 1743−1767.
(35) Davis, J. R. *Corrosion of Aluminum and Aluminum Alloys*; ASM International, 1999, pp 25−49.
(36) Barlag, R.; Nyasulu, F.; Starr, R.; Silverman, J.; Arthasery, P.; McMills, L. *J. Chem. Educ.* **2014**, *91*, 766−768.
(37) Rohaizad, N.; Mayorga-Martinez, C. C.; Novotný, F.; Webster, R. D.; Pumera, M. *Electrochem. Commun.* **2019**, *103*, 104−108.
(38) da Silva, E. T.; Miserere, S.; Kubota, L. T.; Merkoçi, A. *Anal. Chem.* **2014**, *86*, 10531−10534.
(39) Li, Y.; Morel, A.; Gallant, D.; Mauzeroll, J. *Anal. Chem.* **2021**, *93*, 9657−9662.
(40) Strohmeier, B. R. *Surf. Interface Anal.* **1990**, *15*, 51−56.
(41) Barrie, A. *Chem. Phys. Lett.* **1973**, *19*, 109−113.
(42) Rastgar, S.; Pleis, S.; Zhang, Y.; Wittstock, G. *ChemElectroChem* **2022**, *9*, No. e202200004.
(43) Power, G.; Ritchie, I. *Electrochim. Acta* **1981**, *26*, 1073−1078.
(44) Chen, C. H.; Meadows, K. E.; Cuharuc, A.; Lai, S. C.; Unwin, P. R. *Phys. Chem. Chem. Phys.* **2014**, *16*, 18545−18552.
(45) Martins, M. A. G. *IEEE Electr. Insul. Mag.* **2010**, *26*, 7−13.
(46) Owrang, F.; Mattsson, H.; Olsson, J.; Pedersen, J. *Thermochim. Acta* **2004**, *413*, 241−248.
(47) Becerra, H. Q.; Retamoso, C.; Macdonald, D. D. *Corros. Sci.* **2000**, *42*, 561−575.
(48) Tammeveski, K.; Kontturi, K.; Nichols, R. J.; Potter, R. J.; Schiffrin, D. J. *J. Electroanal. Chem.* **2001**, *515*, 101−112.

(49) Kruusenberg, I.; Alexeyeva, N.; Tammeveski, K. *Carbon* **2009**, *47*, 651−658.
(50) Bentley, C. L.; Andronescu, C.; Smialkowski, M.; Kang, M.; Tarnev, T.; Marler, B.; Unwin, P. R.; Apfel, U. P.; Schuhmann, W. *Angew. Chem., Int. Ed. Engl.* **2018**, *57*, 4093−4097.
(51) Zhou, H.; Chhin, D.; Morel, A.; Gallant, D.; Mauzeroll, J. *npj Mater. Degrad.* **2022**, *6*, 1−11.
(52) Verwey, E. *Physica* **1935**, *2*, 1059−1063.
(53) Ghez, R. *J. Chem. Phys.* **1973**, *58*, 1838−1843.
(54) Seyeux, A.; Maurice, V.; Marcus, P. *J. Electrochem. Soc.* **2013**, *160*, C189−C196.
(55) Boxley, C. J.; Watkins, J. J.; White, H. S. *Electrochem. Solid-State Lett.* **2003**, *6*, B38−B41.
(56) Cabrera, N.; Mott, N. F. *Rep. Prog. Phys.* **1949**, *12*, 163−184.
(57) Zhang, X. L.; Jiang, Z. H.; Yao, Z. P.; Song, Y.; Wu, Z. D. *Corros. Sci.* **2009**, *51*, 581−587.
(58) Lin, C. F.; Hebert, K. R. *J. Electrochem. Soc.* **1990**, *137*, 3723.
(59) Takahashi, H.; Kasahara, K.; Fujiwara, K.; Seo, M. *Corrosion Sci.* **1994**, *36*, 677−688.
(60) Despić, A.; Radošević, J.; Dabić, P.; Kliškić, M. *Electrochim. Acta* **1990**, *35*, 1743−1746.
(61) Lin, C. F.; Porter, M. D.; Hebert, K. R. *J. Electrochem. Soc.* **1994**, *141*, 96−104.
(62) Moon, S.-M.; Pyun, S.-I. *Corros. Sci.* **1997**, *39*, 399−408.
(63) Nişancioğlu, K.; Holtan, H. *Electrochim. Acta* **1979**, *24*, 1229−1235.
(64) Gudić, S.; Radošević, J.; Smoljko, I.; Kliškić, M. *Electrochim. Acta* **2005**, *50*, 5624−5632.
(65) Szklarska-Smialowska, Z. *Corrosion Sci.* **1999**, *41*, 1743−1767.
(66) Evangelisti, F.; Stiefel, M.; Guseva, O.; Partovi Nia, R.; Hauert, R.; Hack, E.; Jeurgens, L. P. H.; Ambrosio, F.; Pasquarello, A.; Schmutz, P.; Cancellieri, C. *Electrochim. Acta* **2017**, *224*, 503−516.
(67) Hassel, A. W.; Lohrengel, M. M. *Electrochim. Acta* **1995**, *40*, 433−437.
(68) Sato, N. *Electrochim. Acta* **1971**, *16*, 1683−1692.

https://doi.org/10.1021/acs.analchem.2c02459
Anal. Chem. 2022, 94, 14603−14610